LETTERS

A lever-arm rotation drives motility of the minus-end-directed kinesin Ncd

Nicholas F. Endres[1], Craig Yoshioka[2], Ronald A. Milligan[2] & Ronald D. Vale[1]

Kinesins are microtubule-based motor proteins that power intracellular transport[1,2]. Most kinesin motors, exemplified by Kinesin-1, move towards the microtubule plus end, and the structural changes that govern this directional preference have been described[3–5]. By contrast, the nature and timing of the structural changes underlying the minus-end-directed motility of Kinesin-14 motors (such as *Drosophila* Ncd[6,7]) are less well understood. Using cryo-electron microscopy, here we demonstrate that a coiled-coil mechanical element of microtubule-bound Ncd rotates ~70° towards the minus end upon ATP binding. Extending or shortening this coiled coil increases or decreases velocity, respectively, without affecting ATPase activity. An unusual Ncd mutant that lacks directional preference[8] shows unstable nucleotide-dependent conformations of its coiled coil, underscoring the role of this mechanical element in motility. These results show that the force-producing conformational change in Ncd occurs on ATP binding, as in other kinesins, but involves the swing of a lever-arm mechanical element similar to that described for myosins.

Crystal structures of the Ncd dimer show a coiled coil extending directly from the pair of catalytic cores (termed the 'neck')[9–11], and mutagenesis experiments indicate that the proximal portion of the neck functions as the mechanical element that powers minus-end-directed motility[9,12]. Previous cryo-electron microscopy (cryo-EM) studies of dimeric Ncd suggested that the neck extends towards the microtubule plus end in the nucleotide-free, microtubule-bound complex. This assignment was based on the position of an amino-terminal Src homology domain 3 (SH3) domain used as a marker for the neck, because the neck itself was not visible in this study[13]. Neither the neck nor the SH3 marker was observed in the presence of AMPPNP, however, which led to the proposal that ATP binding causes the Ncd neck to transition into a detached and mobile state and that the shift in the average position of this mobile neck towards the microtubule minus end is the driving force for Ncd motility[13]. A conflicting model of the nature and timing of the power stroke has been proposed on the basis of the crystal structure of a motility-deficient Ncd point mutant (NcdN600K)[10], which shows the neck in a different orientation that is predicted to point towards the microtubule minus end. It has been proposed that this structure represents the nucleotide-free state of the motor and that a minus-end-directed power stroke occurs on release of ADP. Thus, the exact nature and timing of the motility-producing conformational change in Ncd remains uncertain.

Here we have used cryo-EM to investigate the position of the neck in dimeric Ncd (residues 281–700; see Methods) bound to a microtubule in the absence of nucleotide and in the presence of two mimics of an ATP-like state, AMPPNP (a non-hydrolysable ATP analogue) and ADP-AlF_4^- (a transition-state analogue). Helical image analysis of 15 protofilament microtubules was used to calculate three-dimensional (3D) density maps (Fig. 1a–c and Methods). All three maps show two distinct globular domains of similar size and shape, which represent the two heads of the Ncd dimer. As seen before[14–16], only one of the two Ncd heads interacts with the microtubule. In the nucleotide-free state, an elongated density emerges from between the two heads of the Ncd dimer, and its length (~65 Å) matches the expected length of the portion of the Ncd coiled coil that emerges beyond the motor domain. This same elongated density was observed in constructs with two different N-terminal tags (SH3 domain, Fig. 1; or His_6, Supplementary Fig. 1), indicating that the density was not an artefact created by a particular tag. In contrast to the previous cryo-EM study, which did not visualize the neck directly[13] and has been subject to re-interpretation[10], the clear connection of the neck density to the Ncd heads in our maps allows us to conclude unambiguously that the Ncd neck is pointing towards the plus end of the microtubule in the nucleotide-free state.

Our cryo-EM maps show a markedly different conformation of the Ncd motor in the presence of ATP analogues. With AMPPNP, the neck and unbound head of Ncd are rotated by ~70° towards the minus end of the microtubule relative to their positions in the nucleotide-free state, whereas the position of the bound head remains unchanged (Fig. 1b; see Supplementary Fig. 2 for difference maps). The neck density is slightly weak, which may reflect either the data quality or some conformational flexibility, but it can be clearly observed projecting from the two heads of the dimer. In the ADP-AlF_4^- map, the neck density is stronger and better defined (Fig. 1c). Despite these variations, an overlay of the two maps shows that the orientation of the heads and neck are identical in the AMPPNP and ADP-AlF_4^- states (Supplementary Fig. 2). Thus, our data indicate that the Ncd neck has a preferred minus-end-pointing position in the ATP-like states and is not completely random in the ATP-like states of the cycle as has been suggested[13]. These results indicate that ATP binding causes a ~70° rotation of the neck and unbound head toward the minus end of the microtubule.

We next used a docking approach to examine the relationship between the two microtubule-bound states of Ncd observed here and the two published X-rays structure of the Ncd dimer[9,10]. We obtained an excellent fit of the wild-type Ncd/ADP crystal structure into the cryo-EM maps of the nucleotide-free state (Fig. 1d). In particular, the neck of the Ncd/ADP structure occupies the elongated density extending from the two catalytic cores (Fig. 1d), and the known microtubule-binding elements in the bound head are positioned in close proximity to tubulin[15,17] (Supplementary Fig. 3). Keeping the bound head in the same orientation on the microtubule, we docked the crystal structure of the Ncd mutant N600K (NcdN600K)[10] into the maps of the Ncd-microtubule complex in the ADP-AlF_4^- state. This structure fitted reasonably well (Fig. 1e), but was improved by a ~10° rigid-body rotation of the neck and unbound head in the

[1]The Howard Hughes Medical Institute, and the Department of Cellular and Molecular Pharmacology, University of California San Francisco, 600 16th Street, San Francisco, California 94107, USA. [2]Center for Integrative Molecular Biosciences, Department of Cell Biology, The Scripps Research Institute, 10550 North Torrey Pines Road, La Jolla, California 92037, USA.

NcdN600K structure (Fig. 1f). Although this slight difference suggests that the crystal structure of this non-motile Ncd mutant in solution might not be a perfect representation of the conformation of the wild-type motor bound to microtubules, our results argue that the NcdN600K structure closely approximates the microtubule-bound ATP state, rather than the nucleotide-free state as previously suggested[10].

Having successfully visualized nucleotide-mediated conformational changes in wild-type Ncd, we examined an Ncd point mutant N340K (NcdN340K) that can generate motion towards either the plus end or the minus end of microtubules with roughly equal probability[8]. Because the structural basis of such bidirectional transport remains unresolved, we examined the NcdN340K–microtubule complex in different nucleotide states. In the density maps of NcdN340K in its nucleotide-free state (Fig. 1g), the shape of the unbound head is not as well defined as it is in the maps of the wild-type motor, and an elongated neck density is not observed. However, an additional disconnected density is observed at the position occupied by the N-terminal end of the neck in the wild-type motor (highlighted in Fig. 1g). One possible interpretation of this density is that the neck and unbound head in the mutant Ncd dimer occupy both the pre-stroke and post-stroke positions in the nucleotide-free state and that the 3D map reflects an average of these two positions. Consistent with this notion, averaging the wild-type nucleotide-free and ADP-AlF_4^- maps yielded a less well-defined unbound head and a disconnected neck density, similar to that seen in the NcdN340K nucleotide-free map (Fig. 1i).

In the NcdN340K/AMPPNP (Supplementary Fig. 4) and NcdN340K/ADP-AlF_4^- (Fig. 1h) maps, the neck density is completely absent, indicating an unstable neck position, and the detached head is also poorly defined (comparisons of NcdN340K/ADP-AlF_4^- and NcdN340K/AMPPNP maps show no significant differences; Supplementary Fig. 4). These data suggest a possible model of the bidirectional motion in which the mutant motor begins its ATPase cycle by binding to a microtubule with its neck oriented either towards the minus end or the plus end, and then adopts a conformationally averaged midpoint position after ATP binding. In this model, the initial direction of movement would be stochastically determined, but once motion begins in a particular direction it could continue in the same direction by virtue of cooperative effects of an ensemble of motors.

Our cryo-EM experiments suggest that Ncd uses its neck as a lever arm to generate a minus-end-directed power stroke in a manner similar to the rotation of the light-chain-binding domain in myosin II. For a lever-arm mechanism, the velocity of the motor should be proportional to the length of its lever arm[18]. Consistent with this prediction, a series of successive neck truncations caused a progressive decrease in velocity in a microtubule-gliding assay, but did not affect enzymatic turnover (ATPase catalytic rate constant, k_{cat}; Fig. 2a). This finding is consistent with previous work on Ncd truncations[10,19], although ATPase activity was not examined in those studies. Truncation experiments are difficult to interpret, however, because the loss of protein structure could damage motor function in unanticipated ways. We therefore sought to increase

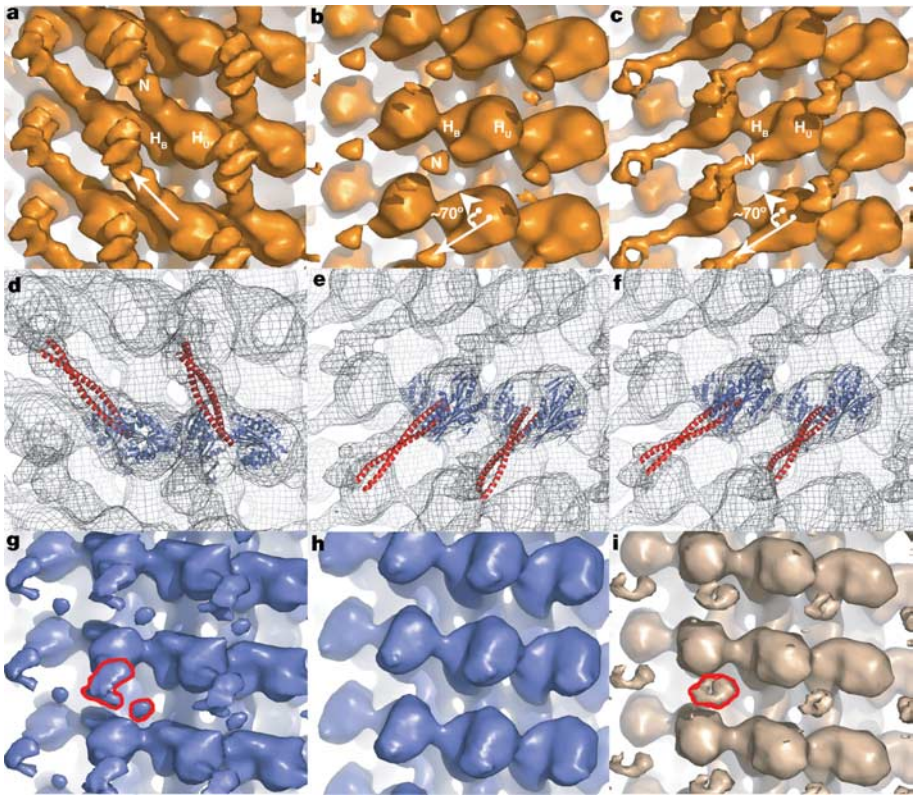

Figure 1 | 3D maps of Ncd–microtubule complexes by cryo-EM. **a**–**c**, Wild-type Ncd in the absence of nucleotide (**a**) and in the presence of the nucleotide analogues Mg^{2+}-AMPPNP (5 mM, **b**) and Mg^{2+}-ADP-AlF_4^- (5 mM, **c**). Putative density for the bound head, unbound head and neck region are marked as H_B, H_U and N, respectively. Arrows indicate the rotation of the unbound head and neck between the nucleotide-free and ATP-like states. **d**–**f**, Ncd crystal structures docked into wild-type maps. Shown is the Ncd-ADP structure[9] docked into the nucleotide-free maps (**d**). The NcdN600K structure[10] (**e**) and the NcdN600K structure with a 10° rotation of the unbound head and neck about Gly 347 (the residue marking the boundary between the neck and the catalytic core) (**f**), are shown docked to the Mg^{2+}-ADP-AlF_4^- maps. **g**, **h**, Cryo-EM maps for the bidirectional mutant NcdN340K, without nucleotide (**g**) and with 5 mM Mg^{2+}-ADP-AlF_4^- (**h**). 5 mM Mg^{2+}-AMPPNP produces an equivalent map to 5 mM Mg^{2+}-ADP-AlF_4^- (Supplementary Fig. 3). **i**, Density map generated by averaging the Ncd wild-type nucleotide-free and Mg^{2+}-ADP-AlF_4^- data. Detached density in NcdN340K nucleotide-free map (**g**) and in Ncd average map (**i**) circled in red. All figures are oriented so that the plus end of the microtubule axis is at the top of the page. Figs were generated with Pymol (Delano Scientific).

velocity by extending the length of the neck with a four-heptad leucine zipper coiled-coil motif ('LZ extension'). As expected for a lever-arm model, fusion of this LZ extension to the native Ncd neck at three different positions increased microtubule gliding velocity without changing ATPase k_{cat} (Fig. 2a). This increase in velocity was not observed when a flexible glycine-serine linker was inserted between the LZ extension and the native Ncd neck (Fig. 2a), suggesting that the LZ extension increases Ncd velocity by extending the length of the mechanical element and not by some other mechanism. The compiled velocity data from the seven truncated or extended neck constructs show that microtubule gliding velocity is proportional to the predicted length of the neck, regardless of whether native or nonnative (LZ extension) residues were used, but ATPase k_{cat} remains unaffected (Fig. 2b, c). Taken together, these data support the notion that a lever-arm rotation of the Ncd neck powers minus-end-directed motility.

A model of Ncd motility invoking the rotation of the neck suggests that the unbound head may not be necessary to generate motility. To test this notion, we prepared a single-headed Ncd heterodimer (N280_Het; Fig. 2a) in which one polypeptide consisted of an intact Ncd catalytic core and neck (residues 280–700) and the second polypeptide consisted of the neck region alone (residues 281–347; Supplementary Fig. 5a and Methods). This motor elicited microtubule gliding at a velocity comparable to that of the normal two-headed Ncd homodimer with a similar ATPase k_{cat} (Fig. 2a). Thus, although our cryo-EM data show that the unbound head rotates along with the neck, the functional data from the heterodimer indicate that contacts between the neck and unbound head are not essential for the mechanism and that the neck alone is sufficient to act as a lever arm. Studies have also shown that a naturally occurring Kinesin-14 heterodimer in yeast (the Kar3p–Cik1p complex, a motor polypeptide in complex with a motor-less coiled coil[20]) is an active, force-producing motor[21,22].

To determine whether the lever-arm motion of the Ncd neck requires a stable coiled-coil interaction, we also tested the motility of an Ncd monomer construct (N325). This construct showed >25-fold reduced motility compared with the single-headed heterodimer, but had an ATPase activity similar to that of the other constructs (Fig. 2a and Supplementary Fig. 5). Thus, a stable coiled coil is required for optimal function of the motor, as would be expected for a lever-arm model.

On the basis of our structural and functional data, we propose the following model of Ncd motility (Fig. 3). Ncd from solution binds to microtubules using one of its heads, triggering ADP release[23]. The excellent fit of the Ncd/ADP structure to the nucleotide-free maps suggests that microtubule binding and ADP release do not produce large-scale conformational changes in the Ncd dimer. Our cryo-EM data suggest that ATP binding leads to a ~70° rigid-body rotation of the neck that produces a minus-end-directed displacement. A subsequent protein isomerization step, possibly before phosphate release, triggers the formation of a weakly bound state and the dissociation of Ncd from the microtubule[24,25]. The neck lever arm can then return to its pre-power stroke position after dissociating from the microtubule, thereby completing the cycle (Fig. 3). Although this overall scheme is supported by our data, questions remain open about the proposed lever-arm mechanism. Specifically, although our data unequivocally show a preferred position of the lever arm in the AMPPNP and ADP-AlF_4^- states, the weaker density in our AMPPNP maps suggests that this post-powerstroke state

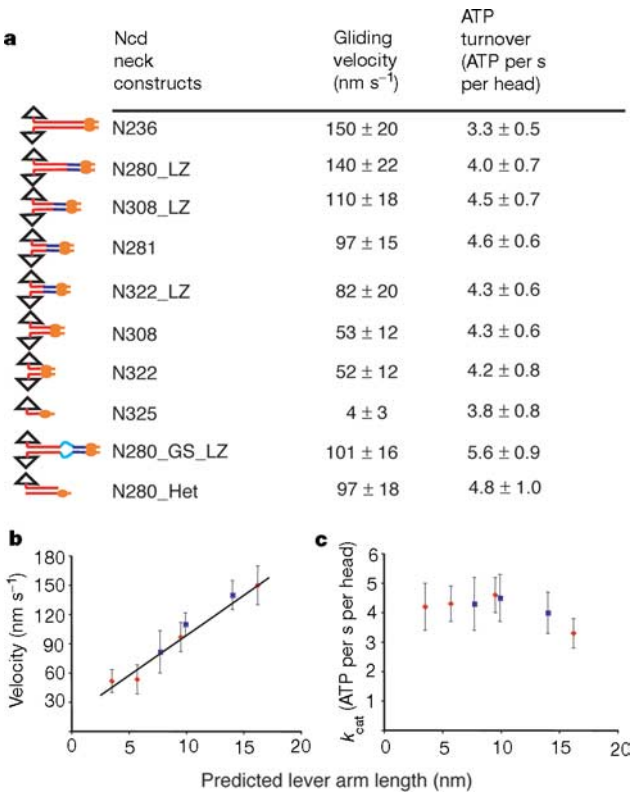

Figure 2 | Ncd mutants with truncated or extended necks. **a**, Gliding assay velocities and ATPase k_{cat} (in ATP molecules per head per s). Velocity data are the mean ± s.d. ($n > 150$); ATPase k_{cat} data are the weighted average and errors obtained from the fits of two independent ATPase experiments from at least two protein preparations. Numbers in the construct name represent the starting residue for the native Ncd residues in the construct. N-terminal LZ extensions (29 residues) and the flexible Gly-Ser linker (12 residues) are labelled LZ and GS, respectively (see Methods). The domain structures of the constructs are shown on the left with motor cores in black, native neck residues in red, LZ extensions in dark blue, the flexible linker in light blue, and the biotin tag in orange. **b**, **c**, Velocities of gliding movement (mean ± s.d; **b**) and ATP k_{cat} (weighted average and errors; **c**) plotted against predicted neck length of each construct. Data points representing constructs containing only native neck residues are red, and data from constructs with LZ extensions are blue.

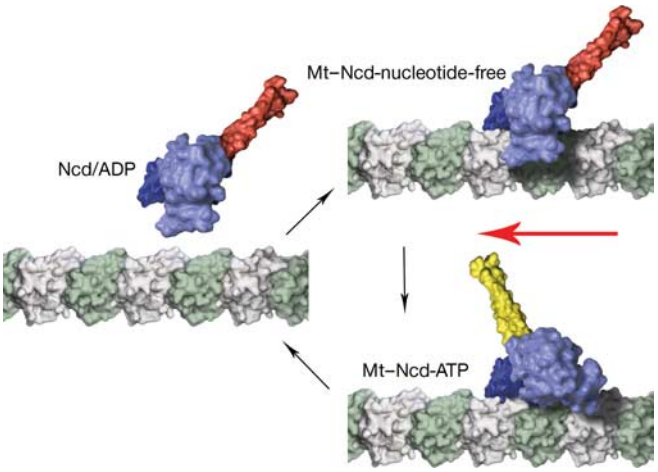

Figure 3 | Model of the Ncd motility cycle. The model is based on surface representations of the docked Ncd structures (Fig. 1d, f). The microtubule is oriented so that the plus end is on the right. In this model, ATP binding causes a rotation of the neck (coloured red in the nucleotide-free and yellow in the ATP state) that leads to a minus-end displacement along the microtubule (indicated by the red arrow). After this lever-arm rotation, the motor releases from the microtubule after nucleotide hydrolysis but probably before phosphate release[24,25]. The released motor then returns to its pre-powerstroke position so that the cycle can repeat. Images rendered from atomic structures by Graham Johnson (fiVth media: ⟨http://www.FiVth.com⟩).

may not be completely rigid and fixed in position, as envisaged by classical swinging crossbridge models of myosin. Future work on this issue will require dynamic measurement of the lever-arm position in different nucleotide states with high spatial and temporal resolution.

Our work shows that the mechanical event in the minus-end-directed Ncd (rotation of the coiled-coil neck) is coupled to the same step of the ATPase cycle (ATP binding) as the mechanical event in the plus-end-directed kinesins (neck linker docking). Thus, reversal of direction in Kinesin-14 motors is accomplished by the evolution of a unique mechanical element that can take advantage of existing conformational changes in the catalytic core, as is also true for direction reversal by the myosin VI motor[26]. Unlike conventional kinesin, which is built for long-distance processive movement, Ncd is a nonprocessive motor[27,28] designed for microtubule crossbridging and tension development in meiotic or mitotic spindles[29]. In this regard, the functions of Ncd are more similar to the tension-generating myosin II motors in muscle. Thus, Ncd and muscle myosin convergently evolved a similar strategy for motility involving a large-scale rotation of an elongated lever and the primary use of only one of the two heads in the motor dimer.

METHODS

Cloning and protein preparation. The constructs used for motility and ATPase assays had an N-terminal pET104 BioEase tag (Invitrogen) for biotinylation and the cryo-EM constructs had an N-terminal SH3 domain cloned from human Nck1 fused to residue 281 of Ncd. All constructs had an N-terminal His_6 tag for purification. The LZ extensions (Fig. 2) contained the yeast GCN4 sequence (VKQLEDKVEELLSKNYHLENEVARLKKLV), and N280_LZ_GS contained a glycine-serine linker (GGGSGGGSGGGS). N280_Het was prepared by coexpressing a biotin- and His_6-tagged neck domain (281–347) with an untagged motor domain (280–700) on the same pET-17b plasmid (Invitrogen) using a single T7 promoter. Proteins were expressed and purified from a Ni^{2+}-NTA agarose column (Qiagen) as described[30]. For motility and ATPase assays, a microtubule affinity purification step, similar to that reported previously[30], was used to select for active motors. N280_Het required an additional gel filtration purification step (Supplementary Fig. 5).

Cryo-EM and helical image analysis. Ncd (4–7 mg ml^{-1}) was dialysed against 25 mM MOPS (pH 7.25), 100 mM NaCl, 2 mM $MgCl_2$, 1 mM EGTA and 1 mM dithiothreitol and was centrifuged (100,000*g*, 15 min) to remove any precipitate. Frozen grids containing microtubules (5 mg ml^{-1}) and Ncd were prepared as described[15] with a final concentration of nucleotide of 5 mM or 1 U of apyrase. Imaging and image analysis were carried out essentially as described[15], with an FEI CM200FEG electron microscope and Gatan cold stage. The number of data sets averaged and the total number of asymmetric units contributing to each 3D map were as follows: Ncd/AMPPNP, 20 data sets, 17,600 particles; Ncd/nucleotide-free, 24 data sets, 17,100 particles; Ncd/ADP-AlF_4^-, 26 data sets, 23,700 particles; Ncd(N340K)/AMPPNP, 20 data sets, 12,150 particles; Ncd(N340K)/AlF_4, 20 data sets, 13,000 particles; Ncd(N340K)/nucleotide-free, 29 data sets, 17,250 particles. For the figures, all 3D data sets were fitted and scaled to a reference created by averaging the microtubule–Ncd/AlF_4^- and microtubule–Ncd/nucleotide-free data (Fig. 1i).

Microtubule gliding and ATPase assays. For gliding assays, glass slides were treated with 0.5 mg ml^{-1} of biotinylated bovine serum albumin (Pierce) and then 0.5 mg ml^{-1} of streptavidin (Pierce) before the motor (200–400 nM for homodimers, 2 μM for heterodimer) was added. Gliding velocities of rhodamine-labelled microtubules were measured as described[30] in motor buffer (25 mM MOPS, 100 mM NaCl, 1 mM EGTA, 2 mM $MgCl_2$ and 5% sucrose; pH 7). ATP hydrolysis rates were measured by an Enzchek assay kit (Molecular Probes) using 10–40 nm of motor and 0–50 μM microtubules in motor buffer with 10 μM paclitaxel and NaCl reduced to 25 mM. Hydrolysis of ATP was plotted against microtubule concentrations, and data were fitted to a Michaelis–Menton equation to determine k_{cat}.

Received 2 September; accepted 23 September 2005.
Published online 28 December 2005.

1. Hirokawa, N. & Takemura, R. Kinesin superfamily proteins and their various functions and dynamics. *Exp. Cell Res.* **301,** 50–59 (2004).
2. Sharp, D. J., Rogers, G. C. & Scholey, J. M. Microtubule motors in mitosis. *Nature* **407,** 41–47 (2000).
3. Rice, S. *et al.* A structural change in the kinesin motor protein that drives motility. *Nature* **402,** 778–784 (1999).
4. Asbury, C. L., Fehr, A. N. & Block, S. M. Kinesin moves by an asymmetric hand-over-hand mechanism. *Science* **302,** 2130–2134 (2003).
5. Yildiz, A., Tomishige, M., Vale, R. D. & Selvin, P. R. Kinesin walks hand-over-hand. *Science* **303,** 676–678 (2004).
6. McDonald, H. B., Stewart, R. J. & Goldstein, L. S. The kinesin-like ncd protein of *Drosophila* is a minus end-directed microtubule motor. *Cell* **63,** 1159–1165 (1990).
7. Endow, S. A., Henikoff, S. & Soler-Niedziela, L. Mediation of meiotic and early mitotic chromosome segregation in *Drosophila* by a protein related to kinesin. *Nature* **345,** 81–83 (1990).
8. Endow, S. A. & Higuchi, H. A mutant of the motor protein kinesin that moves in both directions on microtubules. *Nature* **406,** 913–916 (2000).
9. Sablin, E. P. *et al.* Direction determination in the minus-end-directed kinesin motor ncd. *Nature* **395,** 813–816 (1998).
10. Yun, M. *et al.* Rotation of the stalk/neck and one head in a new crystal structure of the kinesin motor protein, Ncd. *EMBO J.* **22,** 5382–5389 (2003).
11. Kozielski, F., De Bonis, S., Burmeister, W. P., Cohen-Addad, C. & Wade, R. H. The crystal structure of the minus-end-directed microtubule motor protein ncd reveals variable dimer conformations. *Struct. Fold. Des.* **7,** 1407–1416 (1999).
12. Endow, S. A. & Waligora, K. W. Determinants of kinesin motor polarity. *Science* **281,** 1200–1202 (1998).
13. Wendt, T. G. *et al.* Microscopic evidence for a minus-end-directed power stroke in the kinesin motor ncd. *EMBO J.* **21,** 5969–5978 (2002).
14. Hirose, K., Lockhart, A., Cross, R. A. & Amos, L. A. Three-dimensional cryoelectron microscopy of dimeric kinesin and ncd motor domains on microtubules. *Proc. Natl Acad. Sci. USA* **93,** 9539–9544 (1996).
15. Sosa, H. *et al.* A model for the microtubule–Ncd motor protein complex obtained by cryo-electron microscopy and image analysis. *Cell* **90,** 217–224 (1997).
16. Arnal, I., Metoz, F., DeBonis, S. & Wade, R. H. Three-dimensional structure of functional motor proteins on microtubules. *Curr. Biol.* **6,** 1265–1270 (1996).
17. Woehlke, G. *et al.* Microtubule interaction site of the kinesin motor. *Cell* **90,** 207–216 (1997).
18. Uyeda, T. Q., Abramson, P. D. & Spudich, J. A. The neck region of the myosin motor domain acts as a lever arm to generate movement. *Proc. Natl Acad. Sci. USA* **93,** 4459–4464 (1996).
19. Stewart, R. J., Thaler, J. P. & Goldstein, L. S. Direction of microtubule movement is an intrinsic property of the motor domains of kinesin heavy chain and *Drosophila* ncd protein. *Proc. Natl Acad. Sci. USA* **90,** 5209–5213 (1993).
20. Barrett, J. G., Manning, B. D. & Snyder, M. The Kar3p kinesin-related protein forms a novel heterodimeric structure with its associated protein Cik1p. *Mol. Biol. Cell* **11,** 2373–2385 (2000).
21. Sproul, L. R., Anderson, D. J., Mackey, A. T., Saunders, W. S. & Gilbert, S. P. Cik1 targets the minus-end kinesin depolymerase kar3 to microtubule plus ends. *Curr. Biol.* **15,** 1420–1427 (2005).
22. Chu, H. M. *et al.* Kar3 interaction with Cik1 alters motor structure and function. *EMBO J.* **24,** 3214–3223 (2005).
23. Lockhart, A. & Cross, R. A. Origins of reversed directionality in the ncd molecular motor. *EMBO J.* **13,** 751–757 (1994).
24. Pechatnikova, E. & Taylor, E. W. Kinetic mechanism of monomeric non-claret disjunctional protein (Ncd) ATPase. *J. Biol. Chem.* **272,** 30735–30740 (1997).
25. Foster, K. A., Correia, J. J. & Gilbert, S. P. Equilibrium binding studies of non-claret disjunctional protein (Ncd) reveal cooperative interactions between the motor domains. *J. Biol. Chem.* **273,** 35307–35318 (1998).
26. Menetrey, J. *et al.* The structure of the myosin VI motor reveals the mechanism of directionality reversal. *Nature* **435,** 779–785 (2005).
27. deCastro, M. J., Fondecave, R. M., Clarke, L. A., Schmidt, C. F. & Stewart, R. J. Working strokes by single molecules of the kinesin-related microtubule motor ncd. *Nature Cell Biol.* **2,** 724–729 (2000).
28. Pechatnikova, E. & Taylor, E. W. Kinetics processivity and the direction of motion of Ncd. *Biophys. J.* **77,** 1003–1016 (1999).
29. Sharp, D. J., Yu, K. R., Sisson, J. C., Sullivan, W. & Scholey, J. M. Antagonistic microtubule-sliding motors position mitotic centrosomes in *Drosophila* early embryos. *Nature Cell Biol.* **1,** 51–54 (1999).
30. Case, R. B., Pierce, D. W., Hom-Booher, N., Hart, C. L. & Vale, R. D. The directional preference of kinesin motors is specified by an element outside of the motor catalytic domain. *Cell* **90,** 959–966 (1997).

Supplementary Information is linked to the online version of the paper at www.nature.com/nature.

Acknowledgements We thank S. Rice, J. Kardon and J. Ebstein for initial work on this project. This work was supported by NIH grants (to R.D.V. and R.A.M.). Some of the work presented here was conducted at the National Resource for Automated Molecular Microscopy, which is supported by the NIH.

Author Information Reprints and permissions information is available at npg.nature.com/reprintsandpermissions. The authors declare no competing financial interests. Correspondence and requests for materials should be addressed to R.D.V. (vale@cmp.ucsf.edu).